Negative differential resistance in molecular junctions: application to graphene ribbon junctions

Hosein Cheraghchi[1], Keivan Esfarjani[2]
[1] *School of Physics, Damghan University of basic sciences, Damghan, IRAN*
[2] *Department of Physics, University of California, Santa Cruz, CA 95064**
(Dated: April 1, 2018)

Using self-consistent calculations based on Non-Equilibrium Green's Function (NEGF) formalism, the origin of negative differential resistance (NDR) in molecular junctions and quantum wires is investigated. Coupling of the molecule to electrodes becomes asymmetric at high bias due to asymmetry between its highest occupied molecular orbital (HOMO) and lowest unoccupied molecular orbital (LUMO) levels. This causes appearance of an asymmetric potential profile due to a depletion of charge and reduction of screening near the source electrode. With increasing bias, this sharp potential drop leads to an enhanced localization of the HOMO and LUMO states in different parts of the system. The reduction in overlap, caused by localization, results in a significant reduction in the transmission coefficient and current with increasing bias. An atomic chain connected to two Graphene ribbons was investigated to illustrate these effects. For a chain substituting a molecule, an even-odd effect is also observed in the NDR characteristics.

PACS numbers: 73.23.-b,73.63.-b

I. INTRODUCTION

Negative differential resistance (NDR) was first observed by Esaki in diodes[1], where occupied states on one side become aligned with the gap of other side as the voltage is increased. Current reduction also occurs when the position of the resonant states of the molecule move within the gap of one of the contacts[2,3] as in resonant tunneling diodes. In metallic carbon nanotube junctions[4], it was found that the reduction of the current is due to a mismatch in the symmetry of the incoming and outgoing wavefunctions of the same energy. Another work[5] on the I-V characteristic of CoPc on gold has also associated the NDR effect with lack of orbital matching between Ni tip and Co atom. Another origin was explained in STM measurements[6,7]. In this case, narrow peaks in the local density of states (LDOS) of an atomic scale tip sweep past the LDOS of an adsorbed molecule as the bias voltage is increased.

More recently, more instances of NDR were observed[5,8,9] or predicted[10,11,12,13,14,15] in molecular devices. In the case of potential barriers in 2D Graphene sheets[10], the effect was due to the linear dispersion of (massless Dirac) electrons which show a gap in their transmission across the barrier. In Ref. 11 it was due to the presence of Van Hove singularities in the DOS of the 1D electrodes regardless of the type of the contact. This latter explanation is related and similar to that of Refs.[6,7,12] which involves sharp features in the LDOS. In these cases, however, the general conditions necessary for the observation of the effect were not clearly elucidated. Sharp features in the LDOS can lead to NDR[12,16], but it is not a sufficient condition for the observation of NDR, as a reduction in *spatial overlap* of those states is also needed.

The current in nanoscale devices is given by the Landauer formula (see eq. 15) which involves the transmission coefficient given by the product of the local density of states (LDOS) of the left and right electrodes by the off-diagonal matrix elements of the Green's function (GF) connecting the left electrode to the right one (see eq.16). A reduction in the current is caused by a lowering of either term in the transmission coefficient. While NDR in some devices is caused by a lowering of the matrix element of the GF[17], in some other cases it is caused by a reduction in the product LDOS within the energy integration window[5,6,7,12,14,16].

In this paper we explain the reason for occurrence of sharp features in LDOS, and also emphasize that charging effects play an enhancing role in producing NDR in the I-V characteristics of nano-junctions. A large bias causes charge depletion, an asymmetric potential profile, and asymmetric coupling even in a symmetric structure, resulting in a stronger localization of states on different parts of the system, thereby reducing transmission and current.

We consider an atomic carbon chain between two graphene tips as a nano-junction (Fig. 1), albeit all results are generalizable to other types of nano-junctions. Weak contacts between tips and the chain/molecule which usually occur in experiments involving break or molecular junctions, are necessary for causing localized states within the molecular region and observation of NDR. So, we adopt a model in which hoppings to leads are smaller than intramolecular or intralead hoppings. We claim that in molecular junctions where NDR is observed, localization of electronic states within the bias energy window is the dominant cause of reduction in current. The weak bond can play the role of a barrier to localize states within or near the molecule. The purpose of our model is not to make quantitative predictions, but just to illustrate the NDR mechanism using a simple enough model. Given the small size of contact we assume that transport at high bias is mostly coherent and dissi-

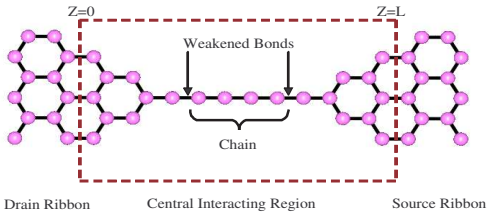

FIG. 1: (Color online) Two Graphene tips connected with a weakened bond to a carbon chain. Tips have sharp structures. The weakened bond is considered to be 0.3 of the normal hopping of the C-C bond. The central interacting region is shown with the dashed rectangle.

pation due to electron-phonon interactions occurs mainly in the drain.

After presenting Hamiltonian of the system in section II, we will introduce the formalism and method used to handle the electrostatics of the problem in the section III. In the Appendix, electrostatic potential calculated by this method is compared with two other methods. We are going over the general formalism used for the calculation of non-linear transport characteristics in section IV. The responsible for current reduction in an atomic chain between two graphene tips which is known to be localization of states induced by charging effects will be presented in the section V.

II. MODEL

The single electron Hamiltonian of the central system (C) including the molecule is

$$H_C = \sum_{i\in C}[\varepsilon_i + u_i^{ext} + W_i]c_i^\dagger c_i + \sum_{<ij>} t(c_i^\dagger c_j + c_i c_j^\dagger) \quad (1)$$

where $c_i^\dagger$ and c_i are respectively the electron creation and annihilation operators on site i of C, and t is the hopping energy between nearest neighbor atoms. One π orbital per site is considered for this system. Under an applied bias, the solution to Poisson's equation is the sum of the solution to *Laplace* with symmetric boundary conditions on the electrodes $V(z=0) = -V/2$ and $V(z=L) = V/2$ (this is denoted by u_i^{ext}), and the *solution to Poisson* with boundary condition $V(z = 0) = V(z = L) = 0$ at both ends (this is denoted by $W_i = \sum_j V_{ij}\delta n_j$). The sum $u^{ext} + W$ clearly satisfies Poisson equation and the proper boundary conditions. Here V_{ij} is the electrostatic Green's function calculated by the method of images, and $\delta n_j = n_j - n_j^0$ is the change in the self-consistent charge n_j from its initial equilibrium zero-bias value.

It should be noted that parts of electrodes (here also called as "tips") have been incorporated inside the interacting central region as there is always some potential drop beyond the contact of the electrodes with the central "molecule".

III. ELECTROSTATIC GREEN'S FUNCTION

The electrostatic potential is determined by both the direct interaction of electrons with each other and the indirect one via image charges. The image charges induced by electrons within the electrodes, strongly depend on the spatial configuration of the electrodes and the contact atoms. For the simplicity of calculations, it is usual to consider the electrodes as two infinite planes perpendicular to the molecule[18]. These planes are located on the contacts.

It is supposed that electrodes are a perfect metal with good screening properties, and that at their boundary the potential can be considered as a constant so that Dirichlet boundary conditions can be applied there. In this case, the potential drop occurs within the central part of the sample, which we call "molecule", although, strictly speaking this central region is taken to be larger than the molecule itself as there is always some potential drop at the contact of the electrodes with the central "molecule".

It should be mentioned that the 3-dimensional Poisson equation needs to be solved in order to find the correct potential profile along the molecule. Indeed the electric field lines are not necessarily straight lines, and a 1D solution would be incorrect. So the Coulomb Kernel needs to be more like the 3-dimensional $1/|r - r'|$ rather than the 1-dimensional $|r - r'|$.

As there is a finite charging energy when the two electrons are on the same site, there should be no divergence in the kernel, and the onsite Coulomb repulsion has been modeled by the so-called "Hubbard" parameter U_H, which could also contain exchange and correlation effects if appropriately chosen. However, image charges potential lowers the potential on one site from its initial value U_H.

In this article, the Ohno-Klopmann (OK) model[19] has been adopted for the Coulombic function U:

$$U(\vec{r}_i, \vec{r}_j) = \frac{1}{\sqrt{|\vec{r}_i - \vec{r}_j|^2 + U_H^{-2}}} \quad (2)$$

It has the correct limits for both large and small interparticle distance $\vec{r}_i - \vec{r}_j$. It has the advantage of including onsite correlations through the Hubbard-like parameter U_H.

In the literature[20], there exists an exact Dirichlet Green's function for a point charge or a distribution of charges between parallel conducting planes held at zero potential. The planes are located at z=0 and z=L. Using this Green function, we present the following exact form which is appropriate for the kernel of Ohno-Klopmann model (Eq.(2)).

$$V(x,y,z;x^{'},y^{'},z^{'}) = 2\int_0^{\infty} dk J_0(\alpha k) f(k,z_<,z_>) \quad (3)$$

where

$$f(k,z_<,z_>) = \frac{\sinh(kz_<)\sinh(k(L-z_>))}{\sinh(kL)} \quad (4)$$

$$\alpha = \sqrt{(x-x^{'})^2+(y-y^{'})^2+U_H^{-2}} \quad (5)$$

The asymptotic behavior of the function $f(k)$ in Eq.(4) is as follows:

$$\lim_{k\to\infty} f(k) \to 0.5e^{-k(z_>-z_<)} \to \begin{cases} 0.5 & z_< = z_> \\ 0 & z_< \neq z_> \end{cases} \quad (6)$$

Moreover, $f(k)$ goes to zero when $k \to 0$. Since at $z_< = z_>$, the function of $f(k)$ will be a constant for $k \gg 1/z_<$, the integration with infinite range can be converted to a limited range integration .

$$V(z_< = z_>) = \frac{1}{\alpha} - \int_0^{k_0} (1-2f(k))J_0(\alpha k)dk \quad (7)$$

where $f(k_0) = 0.5$. The value of k_0 in nanotubes and graphenes used here is about 100. This value depends on the distances between atoms of a molecule and also on the distances between two boundary planes (L). In case of on site electrostatic potential ($x = x^{'}; y = y^{'}$), the first term of Eq.(7) is the Hubbard energy. However, a subtraction term which depends on the distances between atoms and L, lowers the Hubbard energy from U_H. This term is the image charges potential which was considered in the variational method, too (Appendix.B). The value of the semi-empirical Hubbard term for carbon[21], is about 10 eV=0.37 a.u. So $U_H^{-1} \cong 2.72$ whereas the typical bond length is of the order of 1.4 Å=2.6 a.u.

In the Appendix (A,B), we compare this method (namely the exact method) with two other methods so-called the variational and image charges method.

IV. CALCULATION OF CHARGE AND CURRENT

The charge is obtained using the NEGF formalism[22,23]. The electrodes electrochemical potentials and the fermi functions are shown by $\mu_{L,R}$ and $f_{L,R}$, respectively. The retarded Green's function matrix is:

$$G(Z) = [ZI - H - \Sigma_L^r - \Sigma_R^r]^{-1} \quad (8)$$

where $Z = E + i\eta$ is a complex variable whose real part is energy and $\eta \to 0^+$. "I" is the unit matrix. H is the molecule Hamiltonian defined by Eq.(1) in the tight-binding approach. $\Sigma_{L/R}^r$ are the retarded self-energies arising from scattering by the left/right semi-infinite electrodes. These self-energies depend on space configuration of the electrodes and the quality of the electrode-molecule couplings. We have to obtain the surface Green's function of semi-infinite electrodes $g_p(E)$ in order to determine the self-energy. The Lopez-Sancho's method[24] has been used to calculate the surface Green's function. The retarded self-energies are given by:

$$\Sigma_p^r = \tau_p^T g_p^r(E)\tau_p \qquad p \equiv L/R \quad (9)$$

where τ_p is the coupling matrix between the electrodes and the molecule[22]. Since the hopping terms are short-ranged, most elements of the coupling matrix are zero. Broadening of the molecule energy levels due to attachment to the electrodes is related to the self-energies as:

$$\Gamma_p = i[\Sigma_p^r - \Sigma_p^a] = 2\pi\tau_p^T LDOS(p,E)\tau_p \quad (10)$$

Note that the broadenings are proportional to the local density of states at the connecting sites to the electrodes. It should be noted that in this paper transport is assumed to be coherent. The charge density is the sum of two separate parts coming from equilibrium and non-equilibrium charges. Since the voltage division is symmetric on the electrodes, the equilibrium charge n_{eq} is calculated from the retarded Green's function as:

$$n_i^{eq} = \frac{-1}{\pi}\int_{-\infty}^{\mu_0 - V/2} Im[G_{ii}^r(E)]dE \quad (11)$$

where $\mu_0 = \mu_R = \mu_L$. The initial charge n_i^0 is calculated by the above integration in zero bias. In the non-equilibrium situation, the lesser Green's function $-iG^<(E)$ represents the occupation number in the presence of the two electrodes subject to a bias. The non-equilibrium charge n_{non-eq} is determined in the presence of an external bias V.

$$n_i^{non-eq} = \frac{1}{2\pi}\int_{\mu_0 - V/2}^{\mu_0 + V/2} [-iG_{ii}^<(E)]dE \quad (12)$$

It can be simply shown that in the coherent regime the lesser Green's function is determined by the retarded Green's function (Eq.(8)).

$$n_i^{non-eq} = \frac{1}{2\pi}\int_{\mu_0 - V/2}^{\mu_0 + V/2} [G^r(\Gamma_L f_L + \Gamma_R f_R)G^a]_{ii}dE \quad (13)$$

where $f_p = 1/[1+\exp(\frac{E-\mu_p}{k_B T})]$ shows the fermi function of the electrodes. Finally, both parts of the charge are summed to give the total charge:

$$n = n^{eq} + n^{non-eq} \tag{14}$$

Since the molecular Hamiltonian itself depends on the electron density, one needs to do a self-consistent process. The self-consistent algorithm follows these steps. At the first step, the left and right self-energies in Eq.(9) are calculated once before the self-consistent loop. In the second step, the Hamiltonian is set using a guess input charge.

The calculation of charges in Eqs.(11,13) is a hard step as it needs to be well converged. The new and old charges can be mixed with each other by using linear mixing or Broyden's method[25]. Using the mixed charge, this process will start from the first step and continue till convergence is achieved. Finally, having the self-consistent charge and potential profiles, the current passing through the molecule is calculated by the Landauer formula[22].

$$\begin{aligned} I(V) &= \frac{2e}{h}\int_{-\infty}^{\infty} dE\, T(E,V)\,[f_R(E) - f_L(E)] \\ &= \frac{2e}{h}\int_{\mu_0 - V/2}^{\mu_0 + V/2} dE\, T(E,V) \end{aligned} \tag{15}$$

where the second expression is written for zero temperature. The transmission coefficient $T(E,V)$ is defined as:

$$T = \mathrm{Tr}[G^r \Gamma_R G^a \Gamma_L] \propto \mathrm{LDOS}(L)\mathrm{LDOS}(R)|G_{LR}|^2 \tag{16}$$

The integral evaluation for charge density in Eqs.(11,13) has to reach a reasonable accuracy. The speed of the convergence process depends strongly on the accuracy of the integration process. For weak couplings, the van Hove singularities in the density of states (DOS) will make it tremendously difficult to integrate the DOS along the real axis with desired accuracy. Indeed, the singularities arising from the poles of the Green's function are close to the real axis. However, in the complex energy plane, the DOS along the complex contour away from the real axis is very smooth[26]. The resultant formula for a contour integration of the equilibrium charge is:

$$n_i^{eq} = \frac{\rho}{\pi}\int_0^{\pi} Re[G_{ii}(z_0 + \rho e^{i\theta})e^{i\theta}]d\theta \tag{17}$$

$$\rho = \frac{\mu_0 - V/2 - E_{min}}{2}; z_0 = \frac{\mu_0 - V/2 + E_{min}}{2} \tag{18}$$

where E_{min} is chosen to be lower than the lowest eigenvalue of H.

V. RESULTS

Fig.(2) shows the NDR phenomenon in the I-V curves of odd and even length chains located between two graphene tips. To show that NDR is also obtained with gapless leads, we have also made calculations for a (5,5) carbon nanotube and still observed a reduction in the current due to localization of states at the caps of the tubes at high bias. Details will be reported elsewhere. The NDR threshold voltage for odd length chains is higher than that for even chains. The origin of this difference can be traced back to the distance of those levels which play a role in the observation of NDR from the Fermi level. For odd chains, the state at the Fermi level is an extended state over the length of the chain[27], whereas even chains have a gap at the Fermi level. Therefore typically a twice larger bias is needed to observe NDR in odd chains compared to even chains of similar length.

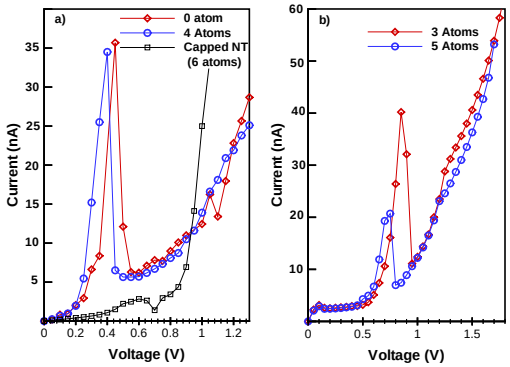

FIG. 2: (Color online) I-V curves for two graphene tips connected to the chain with a) even and b) odd chains. The hopping of the weakened bond is 0.3 times that of the intra-chain hopping (t). In case of "0 atom" where two tips are facing each other with no chain in between, the hopping integral is equal to 0.1 t. NDR is also observed in two (5,5) capped nanotubes (NTs) with a 6 atoms chain in between. Current through NT system is 50 times larger than shown.

To understand the origin of NDR in this system, in Fig. 3 we compare the transmission coefficients at the current peak and valley voltages. As one can see from the figure, there is a large reduction in the transmission of the resonant states when the bias is increased. We will show that the reason for this can be traced back to a loss of LDOS overlap of the left contact with the right one.

In Fig. 4, the electrostatic potential energy and transferred charge ($\delta n = n - n_0$) profiles are plotted for different biases. These distributions are obtained for a small voltage (0.2 V) and voltages of the peak and valley of the current. In the linear regime, potential is nearly symmetric. However, by increasing the bias, some charge is depleted from the source, thereby weakening the effect of screening and enhancing the potential drop further at the source. The asymmetry in the voltage drop can be understood in the following way. The transferred charge between electrodes and molecule depends on the quantum capacitance of the molecule. Quantum capacitance increases with the surface density of states at the source or drain electrochemical potentials. Fig. 5 (a,b)

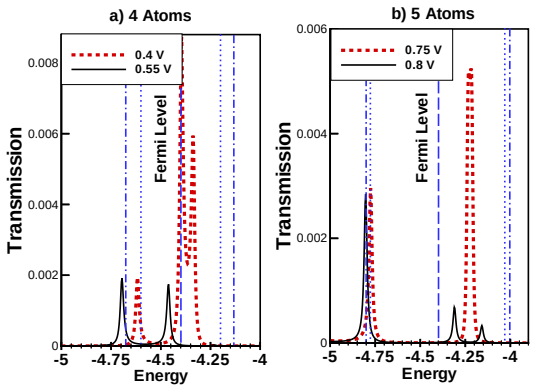

FIG. 3: (Color online) Transmission coefficient through a chain connected to two graphene tips. Transmission is plotted for a chain with a) 4 atoms (even chain) b) 5 atoms (odd chain) at peak and valley voltages. Vertical dashed, dotted and dash-dotted lines identify the Fermi level, integration windows at current-peak voltage and current-valley voltage, respectively. A large reduction in the transmission can be noticed at higher voltage. Transmission through other odd/even chains have similar features.

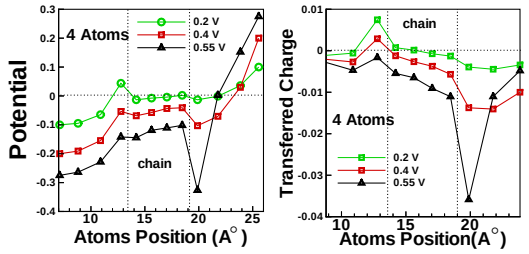

FIG. 4: (Color online) Potential and transferred charge $(n_i - n_i^0)$ for a chain with 4 atoms between two Graphene tips. Profiles for three voltages are plotted; a small voltage, and voltages which correspond to the current peak and valley. Potential and charge has been averaged on each Graphene layer. Source is on the right and drain on the left.

shows that $LDOS(E_F + V/2)$ on the surface layer of the source side is much smaller than $LDOS(E_F - V/2)$ on the drain side. Due to its capacitive coupling with the drain, one state (see Fig. 5(a)) which is localized on the drain side of the molecule is pinned at $E_F - V/2$. So $LDOS(E_F - V/2)$ remains large as the bias is increased, while $LDOS(E_F+V/2)$ gradually decreases when the resonant states in Fig. 5(b) move away from $E_F+V/2$. This asymmetry in LDOS translates into an asymmetry in the couplings of the central region to leads, even though there geometric symmetry is enforced. On the side with weaker coupling (source side in our case) screening would be less effective and potential drop more pronounced. Therefore essentially the asymmetry at large biases develops due to the asymmetry in the distribution of molecular states around the Fermi level. This phenomenon is expected to be universal in molecular double junctions with weak

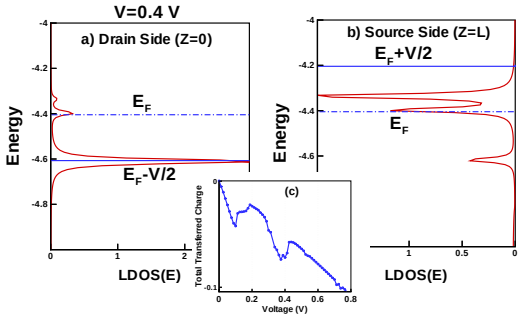

FIG. 5: (Color online) Surface density of states of a) the source and b) drain electrodes on z=0 and z=L shows an asymmetric coupling to the chain. In this case, the chain contains 4 atoms between the two Graphene tips. c) Total charge depletion (δn) of the central region versus applied bias.

couplings. Another consequence of the effective weakening of the couplings to the leads is the sharpening of the molecular states. States near the weak coupling will have narrower peaks at high bias. This is a signature of their enhanced localization.

The strong reduction in the transmission arises from the localization phenomenon which occurs due to the sharp linear potential drop near the source tip. The onsite energies are most negative on the left side while they are most positive on the right side of the source tip (atoms located on 20 and 25A° on Fig. 4). Therefore the LDOS of the left side atoms is large at low energies, whereas that of the right side atoms becomes large at high energies. This situation is very similar to an ionic bond with a large onsite energy difference. The bonding and antibonding eigenstates become farther separated (compared to when onsite energies were equal), and this causes transfer of charge to the low energy site, and enhanced localization of orbitals on the sites due to the large electric field present.

The upper half of each curve in Fig. 6 shows LDOS on the left and right side atoms of the source tip at voltages of the peak and valley of current. It was checked from the LDOS data that states with higher energies become localized on site labeled by 25 Å, while lower energy states become localized on the left atoms of the source tip (site labeled by 20 Å). Therefore the product LDOS at these two sites is reduced with increasing bias, due to a reduced overlap, leading to a decrease in $T(E)$ according to eq.16. In Fig. 6 and for a bias voltage of 0.55 V, strong localization occurs at $E = -4.25eV$ where the transmission is also reduced. The lower half of the curves in Fig. 6 shows that the transmission closely follows the product of LDOS of the left and right atoms (atoms located on 20A° and 25A°) of the source tip. By increasing the bias from the current-peak to current-valley, states with higher energies become localized on the right side of the source tip. So the overlap of LDOS's on the ends of the source tip is reduced. As a result, their product which is proportional to the transmission decreases. If these

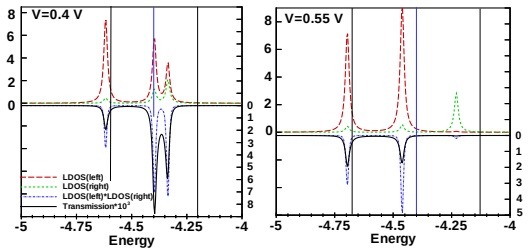

FIG. 6: (Color online) Local density of states on the first (atom located on $20A^\circ$, long dashed line) and last (atom located on $25A^\circ$, dashed line) atoms of the source tip is plotted in upper half of the graphs. Their product (dotted line) is compared with the transmission (solid line) in lower half of the graphs. Voltages are at the current-peak (0.4 V, left) and current-valley (0.55 V, right). The chain connected to the Graphene tips contains 4 atoms. Vertical lines show the Fermi level and the integration window. For comparison with LDOS products, transmission is shown 10^3 times larger.

localized states fall in the integration window of current, transmission as well as current reduction occurs.

VI. CONCLUSION

In conclusion, for observation of NDR, although the presence of sharp features in the density of states located on the sharp tip apexes and their localization is required, the enhancing factor for localization is the charge depletion of the molecule as the bias is increased. Asymmetric potential profile which shows a sharp potential drop in the source side of the molecule, arises from the asymmetry in the LDOS of electrodes connected to the molecule. The asymmetry in LDOS's causes different amounts of charge flow from the molecule to the drain and source electrodes, respectively. The weak screening of the potential due to the depleted charge causes a larger potential drop on the source side. However, the potential on the drain side varies weakly and remains almost flat. Because of the potential drop in the source tip, states with higher energy become localized on the sites with higher potentials (right side of the source tip), and states with lower energy become localized on the sites with lower potentials (left side of the source tip), similar to an ionic bond. The charge depletion and potential drop are intensified in the source tip as the applied voltage is increased. This results in a more effective localization of states. Localization causes a reduction in the overlap of the LDOS's on the ends of the source tip and a subsequent reduction in the transmission and current.

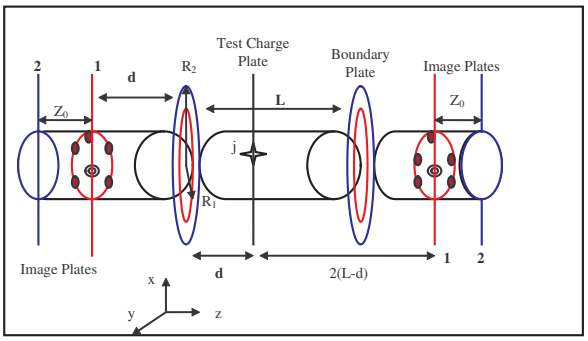

FIG. 7: In the image charges method, test charge induces some image rings just behind the boundary surface.

VII. APPENDIX

A. The variational Method

To find the effect of image charges, we need to impose the Dirichlet boundary condition $V = 0$ at the two left and right electrode planes. Instead of solving Poisson's equation, we postulate the electrostatic Green's function of Eq.(1) to be:

$$V(\vec{r}_i,\vec{r}_j) = \begin{cases} U(\vec{r}_i,\vec{r}_j) - U(\vec{r}_R,\vec{r}_j) & z_i > z_j \\ U(\vec{r}_i,\vec{r}_j) - \frac{U(\vec{r}_R,\vec{r}_j)+U(\vec{r}_L,\vec{r}_j)}{2} & z_i = z_j \\ U(\vec{r}_i,\vec{r}_j) - U(\vec{r}_L,\vec{r}_j) & z_i < z_j \end{cases} \tag{19}$$

where $\vec{r}_R$ and $\vec{r}_L$ show the positions of the atomic layers located in the right and left contact surfaces, respectively. Although this function is not the exact solution of Poisson's equation, it has the correct limits for r_i on the boundary surfaces, where it is equal to zero by construction. It is therefore a reasonable solution in a variational sense, though here we are not varying any parameter to optimize the solution. In this method, we postulate that the image charges potential on the test charge plane ($z_i = z_j$) to be as an interpolation of the left and right solutions in Eq.(19). The kernel used for the coulombic function U has been chosen to be as the OK model in Eq.(2).

B. Numerical Method of Images

The straightforward way for providing an electrostatic Green's function which satisfies Dirichlet boundary condition, is to use image charges. Image charges can be put on fictitious planes just behind the plane on which we want the potential to be zero. Note that the choice of their location or charge is not unique.

Since the potential on the boundary surfaces must be zero, one can find the image charges, if their location is

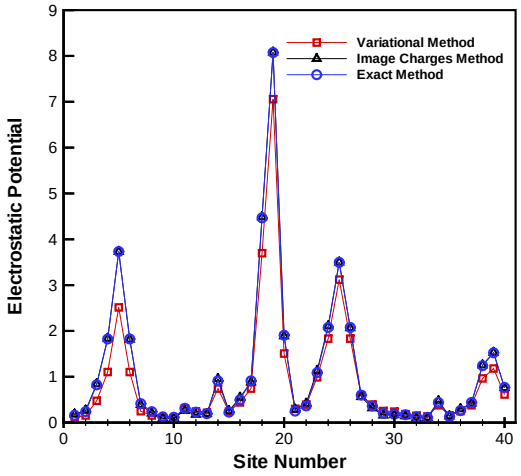

FIG. 8: Comparison of three methods for the calculation of the electrostatic Green function. The sample is a (5,5) nanotube which has 4 rings (40 atoms) in the middle part. The test charge is set on the site number 19. The Hubbard term is considered to be $U_H = 11.3$. Numerical calculation of the image charges method has been done by $n = 20$ and $z_0 = 2$.

fixed, by solving a system of the linear equations. For a test charge located on a molecular site $\vec{r}_j$, one has to solve the set of linear equations which are equal in number to the number of boundary constraints. The constraints leading to a linear system are as follows:

$$V(\vec{r}_i, \vec{r}_j) \;=\; U(\vec{r}_i, \vec{r}_j) + \sum_{k=1}^{n_{img}} q_k^j U(\vec{r}_i, \vec{p}_k^j) \qquad (20)$$

$$V(\vec{r}_L, \vec{r}_j) \;=\; V(\vec{r}_R, \vec{r}_j) = 0 \qquad (21)$$

where $\vec{r}_i$ is the field point and $\vec{r}_j$ is the source point, with its images being of charge q_k^j and located at $\vec{p}_k^j$. For a given test charge location, the number of images n_{img} we need depends on the number of points (constraints) on the boundaries, at which one wants the potential to be zero.

As an example, Fig.(7) shows a nanotube and the position of its contacts and image charges. In this model, all image rings are placed behind the first image plane marked by number 1. The first image charge planes which are the reflected planes from the contact surfaces, are located at $z = -d$ and $z = 2L - d$, where d is the distance of the plane which includes the test charge from the left contact surface. The distance of image planes from each other is considered to be a constant value z_0. The number of image planes is equal to the number of boundary rings (n). It is supposed that the number of sites on an image ring is the same as the boundaries and nanotube rings. In this case, cylindrical symmetry of the images and boundaries sites is important to produce a smooth potential at the boundaries.

Fig.(8) shows a *comparison* between these three methods. A good correspondence can be observed between the potential of image charges method and the exact method. They differ by only 2 percent, while they have about 20 percent difference with the variational method. However, the advantage of the variational method is its simplicity for application on any structure, while the position and values of image charges depend on the structural symmetries.

* Electronic address: cheraghchi@dubs.ac.ir

1 L. Esaki, Phys. Rev. **109**, 603 (1958).
2 R. Tsu and L. Esaki, Appl. Phys. Lett. **22**, 562 (1973).
3 V. J. Goldman, *et al.* Phys. Rev. Lett. **58**, 1256 (1987); T. Rakshit, *et.al.*, Nano. Lett. **4**, 1803 (2004).
4 A.A. Farajian, *et al.* Phys. Rev. Lett. **82**, 5084 (1999).
5 S. Wang, et al. Phys. Rev. B **74**, 195430 (2006).
6 I. W. Lyo, P. Avouris, Science **245**, 1369 (1989)
7 Y. Xue, *et.al.*, Phys. Rev. B. **59** R7852 (1999)
8 T. D. Yuzvinsky,*et.al.*, Nano. Lett. **6**, 2718 (2006)
9 Khoor, *et al.* Bull. APS Meeting, March (2007).
10 D. Dragoman, M. Dragoman, Appl. Phys. Lett. **90**, 143111 (2007).
11 P. Moffatt, E. H. Kim, Appl. Phys. Lett. **89**, 192117 (2006)
12 N. D. Lang, Phys. Rev. B. **55**, 9364 (1997).
13 H. Dalgleish, G. Kirczenow, Phys. Rev. B **73**, 245431 (2006).
14 W. Y. Kim, *et al.* Phys. Rev. B **76**, 033415 (2007).
15 B. Muralidharan, S. Datta, Phys. Rev. B **76**, 035432 (2007).
16 B. Larade, *et al.* Phys. Rev. B. **64**, 75420 (2001).
17 This is due to either a symmetry mismatch between left and right wavefunctions(see for example refs. [4,5], or an exponential decay versus length of the GF due to energy non-alignment (for example in RTD diodes[1,2,3]).
18 V. A. Sablikov, S. V. Polyakov, M. Buttiker, Phys. Rev. B. **61**, 13763 (2000); V. A. Sablikov, B. S. Shchamkhalova, Phys. Rev. B. **58**, 13847 (1998).
19 The potential $V(r) = [r^2 + U_H^{-2}]^{-1/2}$ which has the correct asymptotic behavior at small and large distances is used instead of the Coulomb kernel. It has the advantage of including onsite correlations through the Hubbard-like parameter U_H. K. Ohno, Theor. Chim. Acta **2**, 219 (1964); G. Klopman, J. Am. Chem. Soc. **86**, 4550 (1964).
20 J. D. Jackson, *Classical Electrodynamics*, 3 nd Ed , p140, problem 3.17.
21 K. Esfarjani and Y. Kawazoe, J. Phys.: Cond. Matt. 10, 8257 (1998).
22 S.Datta, *Electronic Transport in Mesoscopic Systems* (Cambridge U.P, Cambridge, 1995); S.Datta, *Quantum Transport: Atom to transistor* (Cambridge U.P, Cambridge, 2005)
23 G. C. Liang, *et al.*, Phys. Rev. B. **69**, 115302, sec IIA

(2004).
[24] M. C. Munoz, *et al.*, Prog. Surf. Sci. **26**, 117 (1988); F. Garcia-Moliner and V. R. Velasco, *Theory of Single and Multiple interfaces* (World Scientific, Singapore, 1992).
[25] C. G. Broyden, Math. Comput. **19**, 577 (1965), also See, e.g., K. Ohno, K. Esfarjani, and Y. Kawazoe, *Computational Materials Science from Ab Initio to Monte Carlo Methods* (Springer, Berlin, 1999).
[26] J. Taylor, *et al.* Phys. Rev. B. **63**, 245407 sec. III.A (2001).
[27] H. Cheraghchi, *et al.* Phys. Rev. B. **72**, 174207 (2005)